ChemComm

COMMUNICATION

View Article Online
View Journal | View Issue

Cite this: *Chem. Commun.*, 2024, **60**, 3311

Received 1st February 2024,
Accepted 26th February 2024

DOI: 10.1039/d4cc00510d

rsc.li/chemcomm

1D Pb halide perovskite-like materials for high performance X-ray detection†

Jing Wang,[ab] Jin-Hai Yang,[a] Jie Chen,[ad] Shuai-Hua Wang, *[ad] Yong-Jun Chen*[a] and Gang Xu [acd]

The strategy of bandgap regulation is important for X-ray detection, but has not been reported for 1D Pb halide perovskite materials. In this work, three such materials, 1, 2 and 3, with a tunable bandgap, were fabricated for application in X-ray detection. 3 shows high sensitivity, far superior to commercial X-ray detectors.

X-ray detectors can convert invisible X-rays into quantifiable and transmitted electrical signals. They have attracted research interest in various applications, such as medical imaging, nuclear radiation monitoring, materials characterization in laboratories and industrial quality inspection.[1–3] Designing and developing materials that can effectively respond to X-rays is crucial in this research field.[4–7] Perovskite materials are promising X-ray detection materials due to their large light absorption coefficient, low exciton binding energy, high carrier mobility and simple preparation methods.[8–12] Among them, Pb halide perovskite is a suitable material for X-ray detection. They usually have the following advantages: (1) large atomic number ensures high X-ray absorption; (2) adjustable bandgap is used to optimize the energy resolution of the detector; and (3) high resistivity results in small dark current and noise. For this reason, Pb halide perovskite materials for X-ray detection have attracted high attention from experts in this field.[13–17]

To date, many works have reported inspiring results that demonstrate the potential application of Pb halide perovskite materials in X-ray detection, like (DGA)PbI_4, (EDBE)$PbCl_4$, $CsPbBr_3$, and $(NH_3C_4H_8NH_3)PbI_4$.[18–21] Compared with three-dimensional (3D) perovskite materials, one-dimensional (1D) Pb halide perovskite materials typically have a single carrier transport path, which brings the property of inhibiting ion migration under external stimuli (*e.g.*, X-ray, ultraviolet light, and pressure, *etc.*).[22,23] This characteristic could effectively prevent abnormal phenomena caused by ion accumulation at the device interface, ensuring the normal operation of the detectors.[24] The strategy of bandgap control could effectively regulate the number of electron and hole pairs in materials, which plays an important role in improving X-ray detection performance.[25,26] However, to our knowledge, there have been no reports on the regulation of the bandgap in 1D Pb halide perovskite materials for X-ray detection.

Herein, a series of 1D Pb halide perovskite-like materials, $(MPC)_2PbX_4$ (MPC is 6-mercaptopyridine-3-carboxylic acid, X = Cl in **1**, Br in **2** and I in **3**), were prepared. These materials have a narrow bandgap, allowing for precise bandgap control, and were utilized in X-ray detection. In the structure of $(MPC)_2PbX_4$, 1D octahedral inorganic anion layer $[PbX_6]^{4-}$ and the organic cation layer are connected by unique hydrogen bonds (N–H···X, O–H···O). These hydrogen bonding interactions enhance the stability of the materials, facilitating the preparation of single crystals. More importantly, as the halogenate atoms change from Cl to Br to I, the bandgap of the crystals decreases gradually, thus achieving better X-ray detection performance. Among them, **3** exhibits the best performance with the sensitivity of 185 μC Gy^{-1} cm^{-2} and a low detection limit of 0.775 μGy s^{-1}. The excellent X-ray detection performance exhibits superior sensitivity to that of the commercial α-Se and a detection limit that is 6 times lower than the requirement for medical diagnostics.

The single crystals of **1**, **2** and **3** were prepared in a concentrated haloid acid solution through slow temperature cooling technology (details see the ESI†). The photos of the obtained single crystals of **1**, **2** and **3** are shown in Fig. S1 (ESI†). Single crystal X-ray diffraction analysis demonstrates that all three crystals belong to the monoclinic system with a space group of $P2_1/c$ (Table S1, ESI†). The three crystals exhibit similar structures, all of which are typical 1D chain perovskite-like structures (Fig. 1a). An octahedral $[PbX_6]^{4-}$ is formed by each Pb^{2+} to

[a] *State Key Laboratory of Structural Chemistry, and Fujian Provincial Key Laboratory of Materials and Techniques toward Hydrogen Energy, Fujian Institute of Research on the Structure of Matter, Chinese Academy of Sciences, Fuzhou 350002, China. E-mail: shwang@fjirsm.ac.cn, chenyongjun@fjirsm.ac.cn*
[b] *College of Chemistry and Materials Science, Fujian Normal University, Fuzhou, Fujian 350007, China*
[c] *Science & Technology Innovation Laboratory for Optoelectronic Information of China, Fuzhou 350108, China*
[d] *University of Chinese Academy of Science (UCAS), Beijing 100049, China*

† Electronic supplementary information (ESI) available: Experimental details and characterization data as well as the crystallographic data of **1**, **2**, and **3**. CCDC 2314917–2314919. For ESI and crystallographic data in CIF or other electronic format see DOI: https://doi.org/10.1039/d4cc00510d

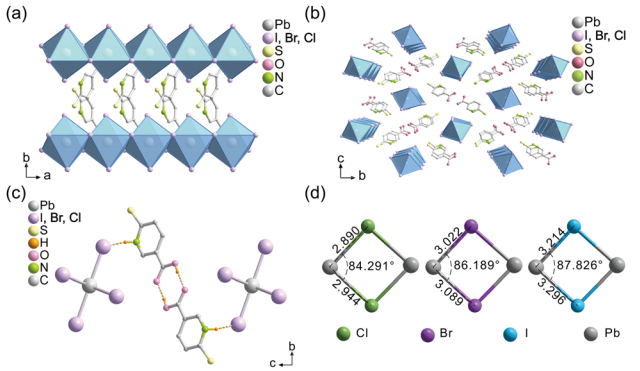

Fig. 1 (a) 1D chain structure of **3**. (b) Bulk structure view of **3** along the *a*-axis. (c) Structure of the hydrogen-bonding network formed. (d) The bond lengths and angles of inorganic components.

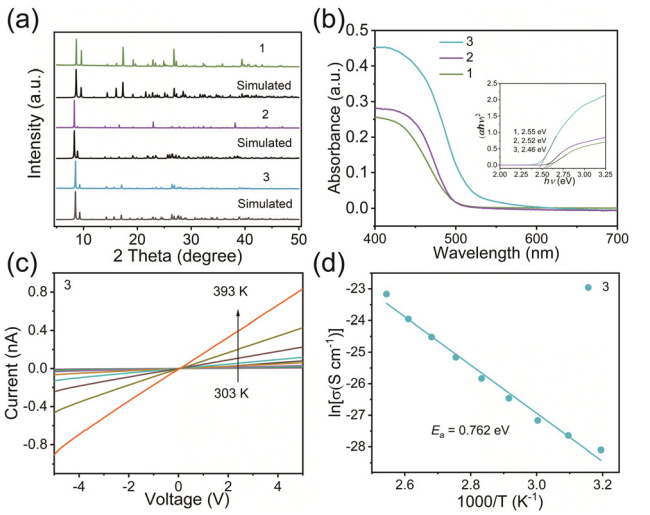

Fig. 2 (a) PXRD patterns of crystals of **1**, **2**, and **3**. (b) UV-Visible absorption spectra of crystals of **1**, **2**, and **3**. (Inset: optical bandgap calculated from the corresponding Tauc plot). (c) Temperature-dependent conductivity of **3**. (d) The linear relationship between ln(σ) of the conductivity of crystal **3** and the reciprocal temperature.

connect with two independent X^- anions and four bridging X^- anions and the inorganic framework extends infinitely with edge-sharing $[PbX_6]^{4-}$ along the crystallographic *a*-axis. The organic cations and inorganic framework were anchored by hydrogen bonds (N–H···X) generated from the N atom and halogen (Fig. 1b and c). This free halogen substitution from Cl to Br to I brings an increase in the bond length and angle of the inorganic octahedra (Fig. 1d). Interestingly, due to the cleavage of disulfide bonds, another stronger hydrogen bond (O–H···O) is formed between the organic cations (Fig. 1c and Tables S2–S4, ESI†). The stronger hydrogen bond may enhance the stability of the crystals, facilitating the successful preparation of single crystals of **1**, **2** and **3**.

To investigate their stability, the crystals of **1**, **2** and **3** were successfully prepared and certified by the powder X-ray diffraction (PXRD) tests. The PXRD patterns of all crystals exhibit well-matched curves to the simulated ones, indicating the absence of any impure phase (Fig. 2a). The thermal and chemical stabilities of the single crystals were explored (for details see Fig. S2 and S3, ESI†). The series of Pb halide perovskite-like materials exhibits good stability, which is attributed to the unique hydrogen bonding (N–H···X, O–H···O). The high stability of the crystals sets a fundamental basis for further application.

Density functional theory (DFT) theoretical calculations revealed that crystal **3** possesses a direct bandgap structure with a narrow bandgap of 2.16 eV (Fig. S4, ESI†). Based on this, the bandgap structure of this series of 1D Pb halide perovskite-like materials was explored through UV-Visible absorption spectrum. The bandgap values of this series of crystals were calculated *via* the Tauc plot, which are 2.55 (**1**), 2.52 (**2**) and 2.46 (**3**) eV, respectively (Fig. 2b). As the halogen is replaced from Cl to Br to I, the bandgap gradually decreases. The reduced bandgap brings higher electron mobility and stronger light absorption, which improves its optoelectronic performance (detail see Fig. S4, ESI†). The bandgaps of **1**, **2** and **3** are within the bandgap range of semiconductors (1–3 eV), implying that this series of 1D Pb halide perovskite-like materials are potential semiconductor materials.[27–29]

To confirm the semiconductor nature of this series of crystals, we explored their electrical properties. The electrical conductions (*I–V* curves) were measured at various temperatures. The crystals of **1**, **2** and **3** exhibit conductivities of 0.01, 0.015 and 0.02 nS cm^{-1} at 303 K, respectively, which increase with rising temperature (Fig. 2c and Fig. S5, ESI†). Through ln(*σ*)-1000/*T* plots fitted to straight lines based on the variant of the Arrhenius equation, the activation energy for charge transport (E_a) of **3** can be estimated to be 0.762 eV (Fig. 2d).[30] Therefore, the temperature-dependent electrical conductivity and suitable optical bandgap indicate that this series of 1D Pb halide perovskite-like materials are semiconductors.

Owing to the impressive semiconducting properties and narrow bandgap of this series of 1D Pb halide perovskite-like materials, we conducted further evaluations on their X-ray detection performance. As shown in Fig. 3a and Fig. S6 (ESI†), the resistivity of **1**, **2** and **3** were determined to be 4.5×10^{10}, 7.5×10^{9} and 2.5×10^{9} Ω cm, respectively, which is larger than the values previously reported for Pb hybrid perovskites, such as $MAPbX_3$, and $MAPbI_3$.[31–33] This high intrinsic resistivity of this series of crystal materials leads to a low dark and noise current, which is favourable for X-ray detection, greatly increasing the signal-to-noise ratio (SNR) and switching ratio.[34,35] Efficient charge collection is also important for X-ray detection, which can be estimated through the mobility lifetime ($\mu\tau$) product (for details see Fig. S7, ESI†). The crystals of **1**, **2** and **3** exhibit a $\mu\tau$ product of 1.05×10^{-3}, 1.75×10^{-3} and 1.71×10^{-3} cm^2 V^{-1}, respectively (Fig. 3b and Fig. S7, ESI†). They are higher than some reported hybrid perovskites, such as $(PEA)_2PbI_4$ (1.07×10^{-4} cm^2 V^{-1}) and $(CH_3OC_3H_9N)_2PbBr_4$ (8.4×10^{-5} cm^2 V^{-1}), even at least three orders of magnitude larger than commercial α-Se film ≈ 10^{-7} cm^2 V^{-1}.[36,37] Furthermore, the absorption coefficients of **1**, **2** and **3** are higher than that of Si and comparable to the value for α-Se in the entire energy range (Fig. 3c). **3** with the smallest bandgap has a higher absorption coefficient than **1** and **2**. This result suggests that regulating the bandgap can affect the properties of semiconductors, thereby affecting its X-ray detection performance.

The high bulk resistivity, relatively large $\mu\tau$ product and high absorption coefficient make this series of 1D Pb halide perovskite-like materials highly promising for X-ray detection. Here, an X-ray

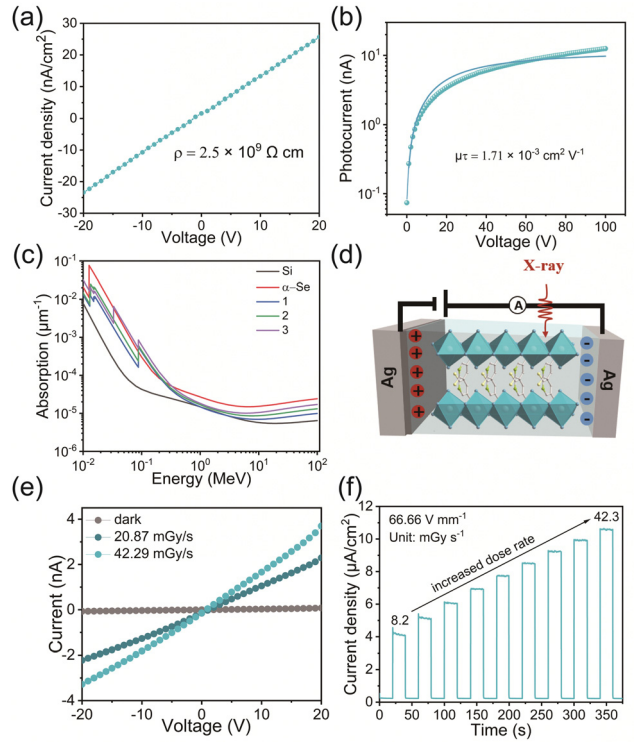

Fig. 3 (a) Bulk resistivity of **3**. (b) The voltage-dependent photoconductivity of **3** under X-ray irradiation. (c) The absorption coefficients of **1**, **2** and **3** and other representative semiconductors *versus* photon energy. (d) Device manufacturing diagram of single crystals. (e) *I*–*V* traces of **3** in the dark and under X-ray irradiation. (f) Photo-responses of **3** to X-rays with increased dose rates.

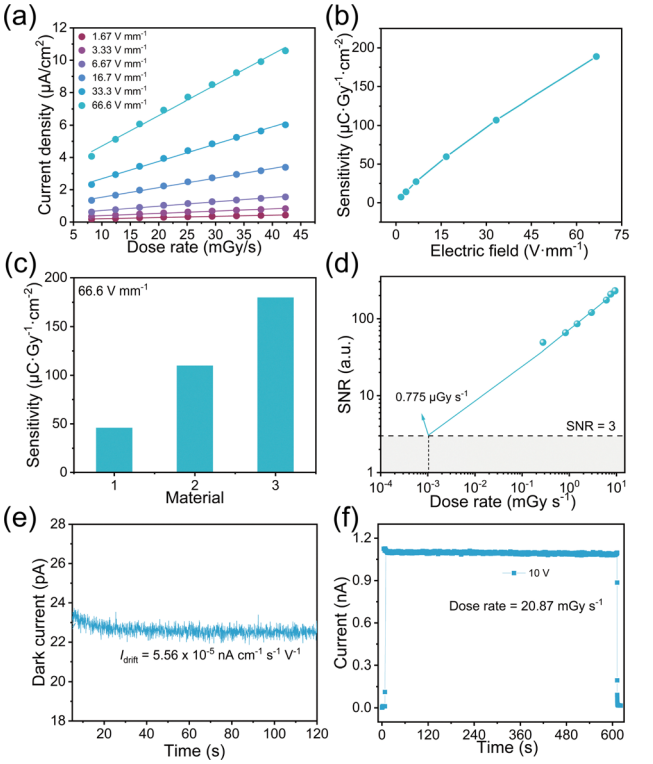

Fig. 4 (a) Linearly fitted current density and X-ray dose rate to obtain sensitivity at different biases. (b) Sensitivity under different electric fields of **3**. (c) Sensitivity comparison of **1**, **2**, and **3**. (d) Signal-to-noise ratio of **3** at 50 V. (e) Dark current drift measurement of **3**. (f) Photocurrent stability of **3** under continuous X-ray irradiation.

detector with a vertical detector structure was fabricated using single crystals of this series of 1D Pb halide perovskite-like materials (Fig. 3d and Fig. S8, ESI†). Fig. 3e demonstrates the *I*–*V* traces of **3** in the dark and under different dose rates of X-ray irradiation, presenting an apparent photocurrent. The current exhibits symmetry for positive and negative voltages, indicating suppressed ion migration in crystals of **3** (Fig. 3e). Similar results of apparent current and symmetric current under positive and negative voltages are also observed in crystals of **1** and **2** (Fig. S9, ESI†). X-ray irradiation was used to induce current responses in single crystal-based detectors of **1**, **2**, and **3** (Fig. 3f and Fig. S10, ESI†). As the X-ray dose rates increased from 8.2 to 42.3 mGy s^{-1} under an electric field of 66.66 V mm^{-1}, the photocurrent densities of **1**, **2** and **3** all presented a remarkable increase. These results reveal the outstanding photoresponse of single crystals **1**, **2** and **3** to X-ray irradiation.

The sensitivity (*S*) is a crucial parameter for evaluating the performance of materials in X-ray detection and is obtained by linearly fitting the correlation between the X-ray dose rate and the photo-current density. The photo-responses of crystals **1**, **2**, and **3** to increasing X-ray dose rates were tested at different electric fields to investigate sensitivity (Fig. 4a and Fig. S11, S12, ESI†). With the increase of the electric field, the sensitivity gradually increases (Fig. 4b and Fig. S11, S12, ESI†). The crystals of **1**, **2** and **3** exhibit high sensitivity of 60, 120 and 185 μC Gy^{-1} cm^{-2} at the same electric field, as shown in Fig. 4c. Among them, the crystal of **3** has the highest sensitivity. This sensitivity value is comparable to that of some typical 3D Pb hybrid perovskites for X-ray detection, such as $MAPbBr_3$ (80 μC Gy^{-1} cm^{-2}) and $FAPbBr_3$ (169 μC Gy^{-1} cm^{-2}), but is 8 times higher than the commercial X-ray detector of α-Se (20 μC Gy^{-1} cm^{-2} at 100 KV cm^{-1}).[38,39] Furthermore, the detection limits of **1**, **2** and **3** as X-ray detectors were investigated. The International Union of Pure and Applied Chemistry defines that the X-ray dose rate with the SNR of 3 is the detection limit. Through fitting the correlation between SNR and dose rates, the detection limits of **1**, **2** and **3** were determined as 43.5, 8.072 and 0.775 μGy s^{-1}, respectively (Fig. 4d and Fig. S13, ESI†). The detection limit of **3** is 6 times lower than the requirement for medical diagnostics (5.5 μGy s^{-1}).[40] Compared with **1** and **2**, **3** exhibits the lowest detection limit due to its stronger light absorption ability resulting from the minimum bandgap. This highlights the crucial role of bandgap regulation in achieving superior X-ray detection performance (sensitivity and detection limit).

The dark current drift (I_{drift}) is also an important parameter for assessing the stability of devices, which is determined through the following equation (details see Fig. S14, ESI†). As shown in Fig. 4e and Fig. S14 (ESI†), the I_{drift} of single crystals **1**, **2** and **3** were calculated to be 3.31 × 10^{-5}, 6.33 × 10^{-5}, and 5.56 × 10^{-5} nA cm^{-1} s^{-1} V^{-1}, respectively. The I_{drift} values of this series of 1D Pb halide perovskite-like materials are equivalent to some previously reported hybrid perovskites,[41,42] such as $PEA_2MA_8Pb_9I_{28}$ (1.8 × 10^{-5} nA cm^{-1} s^{-1} V^{-1}) and $Cs_2AgBiBr_6$

(7.4×10^{-5} nA cm^{-1} s^{-1} V^{-1}), indicating the excellent stability of the devices. Moreover, **3** with the best X-ray detection performance is selected to investigate the irradiation stability. The **3** based X-ray detector was exposed to continuous X-ray irradiation of 20.87 mGy s^{-1} under 10 V (Fig. 4f). Following a total X-ray dose rate of 12.522 Gy, there is no obvious change of photocurrent and dark current, highlighting its outstanding irradiation stability. These results indicate the excellent irradiation stability of this series of 1D Pb halide perovskite-like materials.

In summary, a series of 1D Pb halide perovskite-like materials with a tunable bandgap have been fabricated successfully to apply in X-ray detection for the first time. As predicted, X-ray detection performance increases gradually as the bandgap decreases from **1** to **2** to **3**. It is worth noting that **3** demonstrates the best performance with a sensitivity of 185 μC Gy^{-1} cm^{-2} and a low detection limit of 0.775 μGy s^{-1}, which is 6 times lower than the requirement for medical diagnostics. Additionally, these crystals exhibit exceptional irradiation stability. This work sheds light on future explorations of high-performance X-ray detection based on low dimensional perovskite-like materials.

J. W., Y.-J. C., S.-H. W. and G. X. conceived the idea. J. W. and J.-H. Y. designed the experiments, and collected and analysed the data. J. C. assisted with the experiments and characterization. J. W., Y.-J. C. and S.-H. W. wrote the manuscript. All authors discussed the results and commented on the manuscript.

This work financially supported by the National Natural Science Foundation of China (91961115, 22325109, 22171263, and 62227815), Scientific Research and Equipment Development Project of CAS (YJKYQ20210024), Fujian Science & Technology Innovation Laboratory for Optoelectronic Information of China (2021ZR101), the Natural Science Foundation of Fujian Province (2021J02017), Self-deployment Project Research Program of Haixi Institutes, Chinese Academy of Sciences (CXZX-2022-GH09) and Project Funded by China Postdoctoral Science Foundation (2023M743496). In addition, thanks are extended for the single crystal preparation and analysis assisted by Lei Wang and Prof. Lina Li from the Fujian Institute of Research on Structure of Matter, Chinese Academy of Sciences.

Conflicts of interest

There are no conflicts to declare.

Notes and references

1 R. Zhuang, X. Wang, W. Ma, Y. Wu, X. Chen, L. Tang, H. Zhu, J. Liu, L. Wu, W. Zhou, X. Liu and Y. Yang, *Nat. Photonics*, 2019, **13**, 602.
2 C. Bao, J. Yang, S. Bai, W. Xu, Z. Yan, Q. Xu, J. Liu, W. Zhang and F. Gao, *Adv. Mater.*, 2018, **30**, 1803422.
3 Y. Zhou, J. Chen, O. M. Bakr and O. F. Mohammed, *ACS Energy Lett.*, 2021, **6**, 739–768.
4 H. Li, J. Li, N. Shen, S. Chen, H. Wei and B. Xu, *Nano Energy*, 2024, **119**, 109055.
5 M. Kodur, R. E. Kumar, Y. Luo, D. N. Cakan, X. Li, M. Stuckelberger and D. P. Fenning, *Adv. Energy Mater.*, 2020, **10**, 1903170.
6 H. Kim, J. S. Han, J. Choi, S. Y. Kim and H. W. Jang, *Small Methods*, 2018, **2**, 1700310.
7 C. Ma, D. Shen, M.-F. Lo and C.-S. Lee, *Angew. Chem., Int. Ed.*, 2018, **57**, 9941–9944.
8 J. Zhou and J. Huang, *Adv. Sci.*, 2018, **5**, 1700256.
9 W. Liu, T. Shi, J. Zhu, Z. Zhang, D. Li, X. He, X. Fan, L. Meng, J. Wang, R. He, Y. Ge, Y. Liu, P. K. Chu and X.-F. Yu, *Adv. Sci.*, 2022, **10**, 2204512.
10 H. Wei and J. Huang, *Nat. Commun.*, 2019, **10**, 1066.
11 W. Qian, X. Xu, J. Wang, Y. Xu, J. Chen, Y. Ge, J. Chen, S. Xiao and S. Yang, *Matter*, 2021, **4**, 942–954.
12 T. Chen, X. Li, Y. Wang, F. Lin, R. Liu, W. Zhang, J. Yang, R. Wang, X. Wen, B. Meng, X. Xu and C. Wang, *J. Energy Chem.*, 2023, **79**, 382–389.
13 C. Zhou, M. Han, Y. Xiao, W. Tan, X. Jin, X. Wu, Y. Yang, S. Zhu, H. Lin, S. Lin, Q. Chen, Q. Liang, J. Hu, W. Zhang and Y. Jiang, *Mater. Sci. Eng.*, 2023, **156**, 100756.
14 P. Jin, Y. Tang, X. Xu, P. Ran, Y. Wang, Y. Tian, Y. Huang, B. Zhu and Y. Yang, *Small Methods*, 2022, **6**, 2200500.
15 J. Di, H. Li, L. Chen, S. Zhang, Y. Hu, K. Sun, B. Peng, J. Su, X. Zhao, Y. Fan, Z. Lin, Y. Hao, P. Gao, K. Zhao and J. Chang, *Research*, 2022, **2022**, 9768019.
16 Z. Xu, X. Liu, Y. Li, X. Liu, T. Yang, C. Ji, S. Han, Y. Xu, J. Luo and Z. Sun, *Angew. Chem., Int. Ed.*, 2019, **58**, 15757–15761.
17 Y. Shen, C. Ran, X. Dong, Z. Wu and W. Huang, *Small*, 2023, **10**, 2308242.
18 B. Zhang, T. Zheng, J. You, C. Ma, Y. Liu, L. Zhang, J. Xi, G. Dong, M. Liu and S. Liu, *Adv. Mater.*, 2023, **35**, 2208875.
19 M. D. Birowosuto, D. Cortecchia, W. Drozdowski, K. Brylew, W. Lachmanski, A. Bruno and C. Soci, *Sci. Rep.*, 2016, **6**, 37254.
20 H. Zhang, F. Wang, Y. Lu, Q. Sun, Y. Xu, B.-B. Zhang, W. Jie and M. G. Kanatzidis, *J. Mater. Chem. C*, 2020, **8**, 1248–1256.
21 Y. Shen, Y. Liu, H. Ye, Y. Zheng, Q. Wei, Y. Xia, Y. Chen, K. Zhao, W. Huang and S. Liu, *Angew. Chem., Int. Ed.*, 2020, **59**, 14896–14902.
22 S. You, P. Yu, J. Wu, Z.-K. Zhu, Q. Guan, L. Li, C. Ji, X. Liu and J. Luo, *Adv. Sci.*, 2023, **10**, 2301149.
23 X. Xu, Y. Wu, Y. Zhang, X. Li, F. Wang, X. Jiang, S. Wu and S. Wang, *Energy Environ. Mater.*, 2022, **0**, e12487.
24 M.-M. Lun, C.-Y. Su, J. Li, Q.-Q. Jia, H.-F. Lu, D.-W. Fu, Y. Zhang and Z.-X. Zhang, *Small*, 2023, **19**, e2303127.
25 K. Domanski, J.-P. Correa-Baena, N. Mine, M. K. Nazeeruddin, A. Abate, M. Saliba, W. Tress, A. Hagfeldt and M. Grätzel, *ACS Nano*, 2016, **10**, 6306–6314.
26 C.-F. Wang, H. Li, M.-G. Li, Y. Cui, X. Son, Q.-W. Wang, J.-Y. Jiang, M.-M. Hua, Q. Xu, K. Zhao, H.-Y. Ye and Y. Zhang, *Adv. Funct. Mater.*, 2021, **31**, 2009457.
27 A. Mitrofanov, Y. Berencen, E. Sadrollahi, R. Boldt, D. Bodesheim, H. Weiske, F. Paulus, J. Geck, G. Cuniberti, A. Kuc and B. Voit, *J. Mater. Chem. C*, 2023, **11**, 5024–5031.
28 P.-P. Shi, S.-Q. Lu, X.-J. Song, X.-G. Chen, W.-Q. Liao, P.-F. Li, Y.-Y. Tang and R.-G. Xiong, *J. Am. Chem. Soc.*, 2019, **141**, 18334–18340.
29 X. Li, W. Ke, B. Traore, P. Guo, I. Hadar, M. Kepenekian, J. Even, C. Katan, C. C. Stoumpos, R. D. Schaller and M. G. Kanatzidis, *J. Am. Chem. Soc.*, 2019, **141**, 12880–12890.
30 M. Tiemann, *Chem. – Eur. J.*, 2007, **13**, 8376–8388.
31 M. Tiemann, *Chem. – Eur. J.*, 2007, **13**, 8376–8388.
32 D. Shi, V. Adinolfi, R. Comin, M. Yuan, E. Alarousu, A. Buin, Y. Chen, S. Hoogland, A. Rothenberger, K. Katsiev, Y. Losovyj, X. Zhang, P. A. Dowben, O. F. Mohammed, E. H. Sargent and O. M. Bakr, *Science*, 2015, **347**, 519–522.
33 Z. Li, F. Zhou, H. Yao, Z. Ci, Z. Yang and Z. Jin, *Mater. Today*, 2021, **48**, 155–175.
34 W. Pan, H. Wu, J. Luo, Z. Deng, C. Ge, C. Chen, X. Jiang, W.-J. Yin, G. Niu, L. Zhu, L. Yin, Y. Zhou, Q. Xie, X. Ke, M. Sui and J. Tang, *Nat. Photonics*, 2017, **11**, 726.
35 S. You, Z.-K. Zhu, S. Dai, J. Wu, Q. Guan, T. Zhu, P. Yu, C. Chen, Q. Chen and J. Luo, *Adv. Funct. Mater.*, 2023, **33**, 2303523.
36 B. Zhang, Z. Xu, C. Ma, H. Li, Y. Liu, L. Gao, J. Zhang, J. You and S. Liu, *Adv. Funct. Mater.*, 2022, **32**, 2110392.
37 C. Ji, Y. Li, X. Liu, Y. Wang, T. Zhu, Q. Chen, L. Li, S. Wang and J. Luo, *Angew. Chem., Int. Ed.*, 2021, **60**, 20970–20976.
38 H. Wei, Y. Fang, P. Mulligan, W. Chuirazzi, H.-H. Fang, C. Wang, B. R. Ecker, Y. Gao, M. A. Loi, L. Cao and J. Huang, *Nat. Photonics*, 2016, **10**, 333–339.
39 S. Alghamdi, S. Bennett, C. Crean, J. Ghosh, H. Gibbard, R. Moss, J. Reiss, D. Wolfe and P. Sellin, *Appl. Sci.*, 2022, **12**, 2013.
40 Z. K. Zhu, T. Zhu, J. Wu, S. You, P. Yu, X. Liu, L. Li, C. Ji and J. Luo, *Adv. Funct. Mater.*, 2023, **33**, 2214660.
41 X. He, M. Xia, H. Wu, X. Du, Z. Song, S. Zhao, X. Chen, G. Niu and J. Tang, *Adv. Funct. Mater.*, 2021, **32**, 2109458.
42 B. Yang, W. Pan, H. Wu, G. Niu, J.-H. Yuan, K.-H. Xue, L. Yin, X. Du, X.-S. Miao, X. Yang, Q. Xie and J. Tang, *Nat. Commun.*, 2019, **10**, 1989.

